Error-Tolerant Amplification and Simulation of the Ultrastrong-Coupling Quantum Rabi Model

Ye-Hong Chen,[1,2,3] Zhi-Cheng Shi,[1,2] Franco Nori,[3,4,5] and Yan Xia[1,2,*]
[1]Fujian Key Laboratory of Quantum Information and Quantum Optics, Fuzhou University, Fuzhou 350116, China
[2]Department of Physics, Fuzhou University, Fuzhou 350116, China
[3]Theoretical Quantum Physics Laboratory, RIKEN Cluster for Pioneering Research, Wako-shi, Saitama 351-0198, Japan
[4]Quantum Information Physics Theory Research Team, RIKEN Center for Quantum Computing, Wako-shi, Saitama 351-0198, Japan
[5]Department of Physics, University of Michigan, Ann Arbor, Michigan 48109-1040, USA

(Received 30 January 2024; accepted 18 June 2024; published 18 July 2024)

Cat-state qubits formed by photonic cat states have a biased noise channel, i.e., one type of error dominates over all the others. We demonstrate that such biased-noise qubits are also promising for error-tolerant simulations of the quantum Rabi model (and its varieties) by coupling a cat-state qubit to an optical cavity. Using the cat-state qubit can effectively enhance the counterrotating coupling, allowing us to explore several fascinating quantum phenomena relying on the counterrotating interaction. Moreover, another benefit from biased-noise cat qubits is that the two main error channels (frequency and amplitude mismatches) are both exponentially suppressed. Therefore, the simulation protocols are robust against parameter errors of the parametric drive that determines the projection subspace. We analyze three examples: (i) collapse and revivals of quantum states; (ii) hidden symmetry and tunneling dynamics; and (iii) pair-cat-code computation.

DOI: 10.1103/PhysRevLett.133.033603

Introduction.—The quantum Rabi model (QRM) has been used to describe the dynamics of a wide variety of physical setups [1–3]. Generally, the QRM can be divided into different coupling regimes [4,5], where the most interesting one is the ultrastrong coupling (USC) regime. This is because the USC can open new perspectives for efficiently simulating known effects and observing fundamental phenomena in quantum nonlinear optics [1–6]. These coupling regimes are established when the light-matter interaction energy is comparable to the bare frequencies of the uncoupled systems.

Though the USC regime has been achieved in several systems [7–10], it is still difficult to study unexplored physics and observe its fascinating quantum phenomena at will because the coupling regimes should be implemented in a fully tunable and efficient manner [4,5]. In this respect, proposals in both theory [11–14] and experiments [15–19] for analog quantum simulation [20,21] of the QRM were put forward [4,5]. Researchers can therefore study USC-induced quantum phenomena, such as the asymmetry of the vacuum Rabi splitting [13,16,22,23], nonclassical photon statistics, and superradiance transition [17–19]. For simulating the QRM, additional control fields are usually applied to effectively enhance the ratio between the coupling strength and the bare frequencies in a specific rotating frame to reach the USC regime. However, the simulation protocols [11–21] are sensitive to deviations in these additional drives because projecting the system onto a wrong rotating frame can result in a totally wrong effective Hamiltonian. For instance, in the protocols [12,13,24,25] of squeezing-induced USC, a small deviation in the squeezing strength results in a totally different effective Hamiltonian and breaks the desired dynamical predictions. Similar problems exist in other simulation protocols [21].

For realizing an error-tolerant simulation of the QRM in the USC regime, we propose to use a logic qubit, e.g., the cat-state qubit, instead of a physical qubit. The cat-state qubit [26–30] formed by photonic cat states was introduced for fault-tolerant quantum computing because it is noise biased and experiences only bit-flip noise [31–36]. It can be realized by parametrically driving a Kerr-nonlinear resonator (KNR) [33–38]. The odd and even cat states are two degenerate eigenstates of this parametrically-driven KNR. The coupling between the KNR and a cavity can be linearly enhanced when we treat the KNR as a cat-state qubit, allowing to reach the USC regime. Because the cat-state qubit preserves the noise bias, our simulation protocol is also noise-biased and can exponentially suppress the errors caused by deviations in the parametric drive. As examples, we show how this method can explore the following phenomena in the USC regime: (i) collapse and revivals; (ii) hidden symmetry and tunneling dynamics; (iii) pair-cat-code computation.

Physical model.—As shown in Fig. 1(a), we consider a general physical model of a KNR of frequency ω_{KNR} coupled to a cavity of frequency ω, with coupling strength λ. A two-photon drive (i.e., parametric drive) with amplitude P and frequency ω_p is applied to the KNR.

Thus, working in a frame rotating at half the parametric drive frequency, the Hamiltonian under the rotating-wave approximation becomes

$$\begin{aligned} H &= H_0 + H_{\mathrm{KNR}} + H_{\mathrm{int}}, \\ H_0 &= \Delta a^\dagger a + \delta b^\dagger b, \\ H_{\mathrm{KNR}} &= -Kb^{\dagger 2}b^2 + Pb^{\dagger 2} + P^* b^2, \\ H_{\mathrm{int}} &= \lambda a b^\dagger + \lambda^* a^\dagger b. \end{aligned} \tag{1}$$

Here, $\Delta = \omega - \omega_p/2$ and $\delta = \omega_{\mathrm{KNR}} - \omega_p/2$ are detunings, K is the strength of the self-Kerr nonlinearity. A possible implementation of this Hamiltonian involves superconducting circuits (see the Supplemental Material [39] for details), which have experimentally realized Kerr-cat qubits [35,38] and showed a strong suppression of frequency fluctuations due to $1/f$ noise for the pumped cat [35,42,43].

When the parameters Δ, δ, and λ are far smaller than K and P, we can project the whole system onto the subspace spanned by the eigenstates of H_{KNR} [33,36,37]. Coincidentally, the ground eigenstate of the Hamiltonian H_{KNR} are a set of degenerate eigenstates

$$|\mathcal{C}_\pm^\beta\rangle = \frac{1}{\sqrt{\mathcal{N}_\pm}}(|\beta\rangle \pm |-\beta\rangle), \tag{2}$$

which are separated from the other eigenstates with an energy gap $E_{\mathrm{gap}} \simeq 4K|\beta|^2$ [33], where $\beta = \sqrt{P/K}$ is the complex amplitude of the coherent state $|\beta\rangle$ and $\mathcal{N}_\pm$ are normalized coefficients.

In the limit of $\{\Delta, \delta, \lambda\} \ll E_{\mathrm{gap}}$, if the KNR is initially in the cat-state subspace $\mathcal{C} = \{|\mathcal{C}_\pm^\beta\rangle\}$, its dynamics will be confined to this subspace. The KNR can be seen as a two-level system, i.e., a cat-state qubit as shown in Fig. 1(b). We define the Pauli matrices $\sigma_+ = |\mathcal{C}_-^\beta\rangle\langle\mathcal{C}_+^\beta|$, $\sigma_- = (\sigma_+)^\dagger$, and $\sigma_z = |\mathcal{C}_-^\beta\rangle\langle\mathcal{C}_-^\beta| - |\mathcal{C}_+^\beta\rangle\langle\mathcal{C}_+^\beta|$. Working in the cat-state subspace, the effective Hamiltonian reduces to

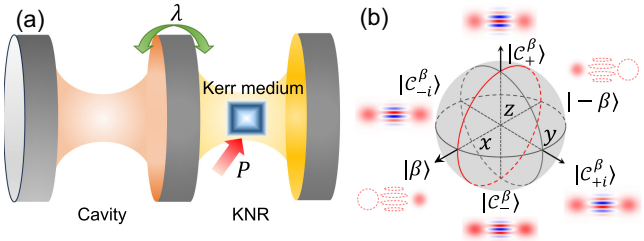

FIG. 1. (a) Schematic of the setup: a parametrically driven Kerr-nonlinear resonator (KNR) is weakly coupled to a cavity with strength λ. (b) Bloch sphere of the cat-state qubit for large β. The red circle denotes the only possible rotation direction for the qubit.

$$H_R = \Delta a^\dagger a + \frac{\tilde{\delta}}{2}\sigma_z + \left[\lambda\beta\left(\frac{\sigma_+}{A} + A\sigma_-\right)a + \mathrm{H.c.}\right], \tag{3}$$

which describes a tunable anisotropic QRM. Here, $A = \sqrt{\tanh|\beta|^2}$ and $\tilde{\delta} = 2\delta|\beta|^2\mathrm{csch}(2|\beta|^2)$. The unitary term $\mathbb{1}_\beta = |\mathcal{C}_-^\beta\rangle\langle\mathcal{C}_-^\beta| + |\mathcal{C}_+^\beta\rangle\langle\mathcal{C}_+^\beta|$ is omitted in Eq. (3). For large β, H_R takes the standard form of the QRM with an enhanced coupling strength $g \simeq \lambda\beta$ because of $A \simeq A^{-1} \simeq 1$. As shown in Fig. 2(a), the effective dynamics governed by the Hamiltonian H coincides very well with that governed by the effective Hamiltonian H_R.

Parameter errors.—In our protocol, there are mainly two errors: (i) driving frequency mismatch described by $\delta_\omega b^\dagger b$; and (ii) driving amplitude imperfections, i.e., deviations in P (or equivalently K). Therefore, the error Hamiltonian is

$$H_{\mathrm{err}} = \delta_\omega b^\dagger b + \delta_P b^{\dagger 2} + \delta_P^* b^2. \tag{4}$$

Projecting onto $\mathcal{C}$, H_{err} becomes

$$H_{\mathrm{err}} \approx \delta_\omega|\beta|^2\begin{pmatrix} A^{-2} & 0 \\ 0 & A^2 \end{pmatrix} + \delta_P(\beta^2 + \beta^{*2})\mathbb{1}_\beta, \tag{5}$$

which is approximatively a unit matrix for large β. As long as $\delta_\omega, \delta_P \ll E_{\mathrm{gap}}$, H_{err} only causes a change in the global phase. We demonstrate this in Fig. 2(b) by illustrating the dynamics governed by the total Hamiltonian $\mathcal{H} = H + H_{\mathrm{err}}$. When the deviations reach $\delta_P = \delta_\omega = \pm 0.1\Delta$, the deviation in the final state population is less than 0.5%.

The effective Hamiltonian in Eq. (3) can be applied to study various physical phenomena. Also, it is easy to achieve some generalizations of the QRM [4,5] by adding additional control fields. The simplest application of our approach is to enhance the coupling in a weak coupling ($g \ll \Delta$) to the USC ($g \gtrsim 0.1\Delta$). The USC regime has a typical dynamical feature, which is called "collapses and revivals" [44]. It describes the appearance of photon-number wave packets that bounce back and forth along

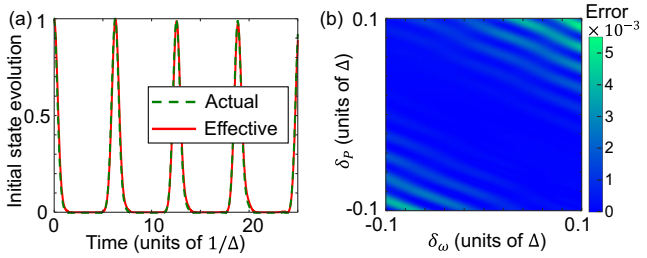

FIG. 2. (a) Time evolutions of the initial state $|0, \mathcal{C}_+^\beta\rangle$ governed by the effective Hamiltonian H_R (red-solid curve) and the Hamiltonian H (green-dashed curve). (b) Deviations in the population of the initial state $|0, \mathcal{C}_+^\beta\rangle$ by adding the error Hamiltonian H_{err} after a finite-time evolution with $t = 4\pi/\lambda$. We choose $\beta = 2$, $K = 10\Delta$, $\lambda = \Delta$, and $\delta = 0.1\Delta$ to reach the USC regime.

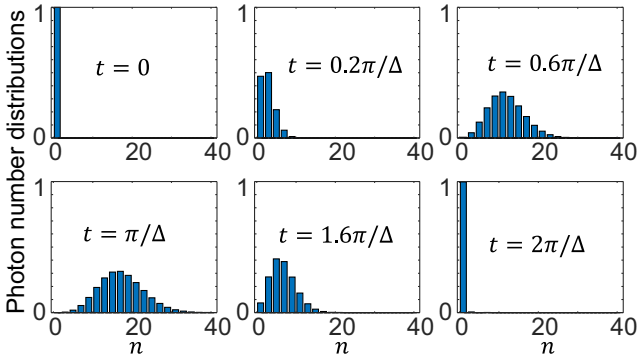

FIG. 3. Instantaneous photon number distribution of the cavity mode a in a finite-time evolution governed by H with the initial state $|0,\mathcal{C}_+^\beta\rangle$, exploring the round trip of a photon number wave packet and collapse revivals. We choose parameters $\beta = 2$, $\lambda = \Delta$, $K = 10\Delta$, and $\delta = 0$.

a defined parity chain, yielding collapses and revivals of the initial population [44]. The parity chain is defined by the parity operator $\Pi = -(-1)^{a^\dagger a}\sigma_z$ with $\Pi|p\rangle = p|p\rangle$ and $p = \pm 1$. For the initial state $|\psi(0)\rangle = |0,\mathcal{C}_+^\beta\rangle$ (corresponding to $p = +1$), in the coupling regime with $g/\Delta \geq 1$ and $\tilde{\delta} = 0$, the coherent evolution of the system results in

$$|\psi(t)\rangle = \exp\left(\frac{i}{\Delta}g^2 t\right)\exp\left[-\frac{i}{\Delta^2}\sin(\Delta t)\right]|\gamma(t),\mathcal{C}_+^\beta\rangle, \quad (6)$$

where $\gamma(t) = (g/\Delta)[\exp(-i\Delta t) - 1]$ is the coherent state amplitude. The revival probability of the initial state is $P_{+0}(t) = |\langle\psi(0)|\psi(t)\rangle|^2 = \exp[-|\gamma(t)|^2]$, which exhibits periodic collapses and full revivals as shown in Fig. 3. This demonstrates that we can effectively achieve the USC using the cat-state qubit.

Hidden symmetry and tunneling dynamics in the asymmetric QRM.—Assuming $|\beta| \geq \sqrt{2}$ and λ are real for simplicity, the asymmetric QRM can be obtained by applying a linear driving $H_a = \Omega(b + b^\dagger)$, with $\Omega \ll E_{\text{gap}}$, onto the KNR, resulting in

$$H_{\text{AR}} \simeq \Delta a^\dagger a + \frac{\tilde{\delta}}{2}\sigma_z + \frac{\epsilon}{2}\sigma_x + g(a^\dagger + a)\sigma_x, \quad (7)$$

where $\epsilon\sigma_x/2$ is the additional asymmetric qubit bias term with $\epsilon = 4\beta\Omega$ and $\sigma_x = \sigma_+ + \sigma_-$. This additional σ_x term breaks the $\mathbb{Z}_2$ symmetry in the standard QRM. Level crossings appear in the spectrum of the asymmetric QRM only if $\epsilon = n\Delta$ $(n = 1, 2, 3, \ldots)$ [45–47]. These level crossings are expected to be associated with some hidden symmetry of the model [45,46]. The origin of this hidden symmetry is established by finding the operators which commute with the asymmetric QRM Hamiltonian at these special values. Such a symmetry is obviously sensitive to deviations in the qubit bias σ_x term. In our protocol, the dominant error Hamiltonian in Eq. (5) does not contain off-diagonal elements (i.e., the σ_x term) because the cat-state qubit preserves the noise bias.

The existence of level crossings is independent of the value of $\tilde{\delta}$ when $\tilde{\delta} \neq 0$. The term $H_t = \tilde{\delta}\sigma_z/2$, leading to transitions between the eigenstates $|\pm x\rangle$ of σ_x, can be regarded as a tunneling term. Removing the tunneling term H_t from H_{AR}, the rest of the Hamiltonian can be analytically solved with eigenstates

$$|n_\pm, \pm x\rangle \simeq D(\pm\alpha)|n\rangle \otimes \frac{1}{\sqrt{2}}(|\mathcal{C}_+^\beta\rangle \pm |\mathcal{C}_-^\beta\rangle), \quad (8)$$

where $D(\pm\alpha) = \exp[\pm\alpha(a - a^\dagger)]$ are displaced operators with amplitude $\alpha = g/\Delta \simeq \lambda\beta/\Delta$, and $|n\rangle$ are the Fock states. The corresponding eigenvalues are $E_n^\pm = n\Delta - g^2/\Delta \pm \epsilon/2$.

Equation (8) shows the eigenstates of two displaced harmonic oscillators with displacing directions determined by the two eigenvalues of σ_x. The asymmetric qubit bias term $\epsilon\sigma_x/2$ lifts the degeneracy and leads to asymmetry in the oscillator potentials [48] as shown in Fig. 4(a). Thus, the levels $|m_+, +x\rangle$ and $|(m+n)_-, -x\rangle$ become degenerate when $\epsilon = n\Delta$. The tunneling process can be reduced to an analytically solvable two-level resonant transition problem [49]. The transition efficiency is determined by the tunneling matrix elements $\langle m_+|(m+n)_-\rangle\tilde{\delta}/2$. However, when ϵ is a non-integer multiple of Δ, e.g., $\epsilon/\Delta \in [0.05, 0.95]$, the transition become off-resonance. Therefore, when $\epsilon/\Delta \in [0.05, 0.95]$, the system mostly remains in its initial state for a long time [see Fig. 4(b)], indicating the tunneling probability decreases. For $m = 0$, a complete population transfer from $|0_+, +x\rangle$ to $|n_-, -x\rangle$ occurs when $\epsilon = n\Delta$, indicating that the tunneling oscillation takes place (see Fig. 5).

Pair-cat code.—Using the bias term $\epsilon\sigma_x/2$ for control, and assuming $\tilde{\delta} = 0$, the lowest two eigenstates in Eq. (8) become degenerate. Their orthogonal basis

$$|\mu_\pm\rangle = \frac{1}{\sqrt{2}}(|\alpha, +x\rangle \pm |-\alpha, -x\rangle), \quad (9)$$

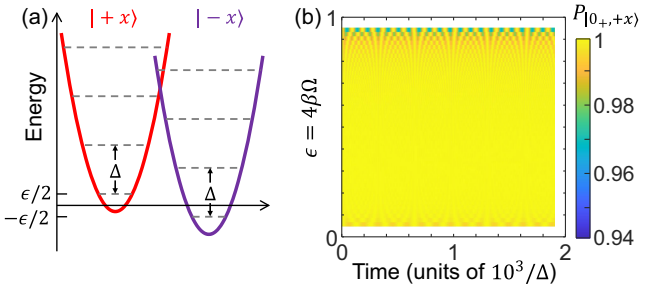

FIG. 4. (a) Schematic effective potentials of the asymmetric QRM for nonzero ϵ, corresponding to a broken $\mathbb{Z}_2$ symmetry. (b) Time evolution governed by H of the initial state $|0_+, +x\rangle$ for $\epsilon \in [0.5, 0.95]$. We choose $\beta = \sqrt{2}$ and $K = 300\Delta$ for the cat-state qubit. Other parameters are $\lambda = 0.5\Delta$ and $\tilde{\delta} = 0.1\Delta$.

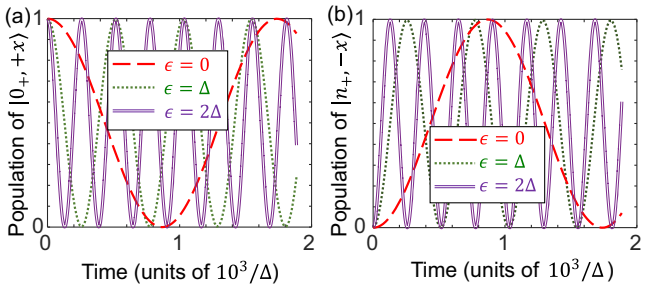

FIG. 5. Populations of (a) the initial state $|0_+,+x\rangle$ and (b) the target states $|n_-,-x\rangle$. For $\epsilon = n\Delta$, the tunneling process is reduced to a two level transition problem, resulting in a Rabi oscillation $|0_+,+x\rangle \leftrightarrow |n_-,-x\rangle$. Parameters are the same as those in Fig. 4(b).

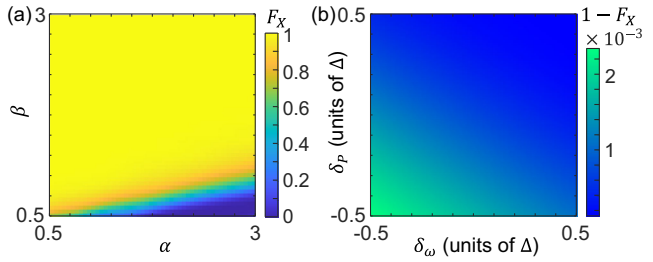

FIG. 6. (a) Average fidelity F_X of the pair-cat-code Paul-X gate versus α and β when $K = 10\Delta$ and $\delta = 0$. (b) Average infidelity $(1 - F_X)$ of the Paul-X gate in the presence of the error Hamiltonian $H_{\rm err}$. We choose $\alpha = \beta$ to be real and $\lambda = \Delta = 0.1$ K to satisfy $\lambda, \Delta \ll E_{\rm gap}$.

are two-mode cat (or, pair-cat) states, which can form a new computational subspace with a code projection

$$P_\mu = |\mu_+\rangle\langle\mu_+| + |\mu_-\rangle\langle\mu_-|. \tag{10}$$

Similar to the single-cat qubits [31,33,37], our pair-cat qubit can also, even more effectively, preserve the noise bias. Focusing on error operators b and $b^\dagger b$, the bias-preserving parameters

$$\begin{aligned}\langle\mu_+|b^\dagger b|\mu_+\rangle - \langle\mu_-|b^\dagger b|\mu_-\rangle &= |\beta|^2 e^{-2|\alpha|^2}(A^{-2} - A^2),\\ \langle\mu_+|b|\mu_-\rangle - \langle\mu_-|b|\mu_+\rangle &= \beta e^{-2|\alpha|^2}(A - A^{-1}),\end{aligned} \tag{11}$$

are exponentially smaller than those of the cat-state qubit:

$$\begin{aligned}\langle\mathcal{C}_+^\beta|b^\dagger b|\mathcal{C}_+^\beta\rangle - \langle\mathcal{C}_-^\beta|b^\dagger b|\mathcal{C}_-^\beta\rangle &= |\beta|^2(A^{-2} - A^2),\\ \langle\mathcal{C}_+^\beta|b|\mathcal{C}_-^\beta\rangle - \langle\mathcal{C}_-^\beta|b|\mathcal{C}_+^\beta\rangle &= \beta(A - A^{-1}).\end{aligned} \tag{12}$$

For operators a and $a^\dagger a$, we have $\langle\mu_+|a|\mu_-\rangle = \langle\mu_-|a|\mu_+\rangle$ and $\langle\mu_+|a^\dagger a|\mu_+\rangle = \langle\mu_-|a^\dagger a|\mu_-\rangle$. These indicate that the pair-cat code can satisfy the Knill-Laflamme condition [50,51] better than the single-cat code regarding single-photon-loss error. Moreover, Eq. (11) demonstrates that a projection of the error Hamiltonian $H_{\rm err}$ onto the pair-cat subspace using P_μ also results in a unit matrix for large α and β. Therefore, the simulated QRM can be a great candidate for realizing fault-tolerant codes tailored to biased-noise qubits.

Paul-X gate.—Noting that a and b are both uncorrectable errors, we can apply the control term $\epsilon\sigma_x/2$ to the system to create an X gate. In the limit $\epsilon \ll E_{\rm gap}$, this additional drive lifts the degeneracy between the states $|\alpha,+x\rangle$ and $|-\alpha,-x\rangle$ and leads to oscillations with an effective Rabi frequency $\epsilon = 4\beta\Omega$ between the states $|\mu_\pm\rangle$. Choosing an evolution time $t_{\rm gate} = \pi/\epsilon$, the evolution operator of the system becomes

$$U_X = |\mu_+\rangle\langle\mu_-| + |\mu_-\rangle\langle\mu_+|, \tag{13}$$

i.e., the Paul-X gate. The average fidelity of the Paul-X gate over all possible initial states can be defined by [52]

$$F_X = \frac{{\rm Tr}(MM^\dagger) + |{\rm Tr}(M)|^2}{d^2 + d}, \tag{14}$$

where $M = \mathcal{P}_c U_X^\dagger U(t_{\rm gate})\mathcal{P}_c$, with $\mathcal{P}_c$ (d) being the projector (dimension) of the computational subspace $\mathcal{C}_\mu = \{|\mu_\pm\rangle\}$. Here, $U(t_{\rm gate})$ is the actual evolution operator calculated for the Hamiltonian H. The gate fidelities calculated for different α and β are shown in Fig. 6(a). As α and β increase, the gate fidelity increases when choosing a fixed Δ. Noting that a larger α corresponds to a larger λ for fixed β, this can lead to infidelity because the condition $\lambda \ll E_{\rm gap}$ cannot be well satisfied. This can cause population leakage out of the computational subspace and reduce the gate fidelity.

The projection of $H_{\rm err}$ onto the pair-cat subspace also results in a nearly unit matrix for large β, indicating the robustness of the pair-cat Paul-X gate against parameter imperfections in P and δ. As shown in Fig. 6(b), the error Hamiltonian $H_{\rm err}$ only causes $\lesssim 0.2\%$ infidelity to the Paul-X gate, even when the deviations δ_P and δ_ω reach $\pm 0.5\Delta$. Moreover, because the bias-preserving parameters in Eq. (11) are exponentially smaller than those in Eq. (12), the influence of $H_{\rm err}$ is also exponentially suppressed in the pair-cat protocol. A comparison [see Fig. 7(a)] between our pair-cat protocol and the single-cat one [35] indicates that our protocol can more efficiently suppress parameter deviations in the parametric drive. Specifically, choosing $\alpha = \beta$, the gate fidelity mostly remains in $F_X \geq 99.95\%$ [black-hollow curve in Fig. 7(a)].

Decoherence.—In the presence of single-photon losses and dephasing, the system dynamics is described by the Lindblad master equation

$$\dot\rho = -i[H,\rho] + \sum_{j=a,b}\kappa_j\mathcal{D}[j]\rho + \kappa_j^\phi\mathcal{D}[j^\dagger j]\rho, \tag{15}$$

where $\mathcal{D}[o]\rho = o\rho o^\dagger - (o^\dagger o\rho + \rho o^\dagger o)/2$ is the standard Lindblad superoperator and κ_j (κ_j^ϕ) is the single-photon loss

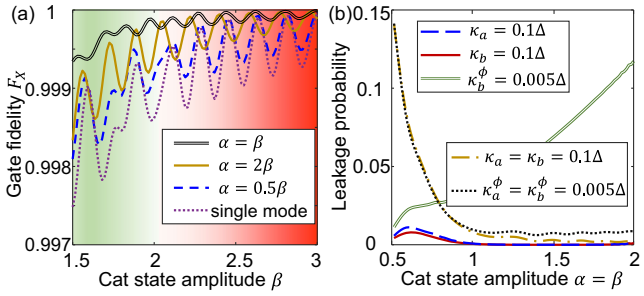

FIG. 7. (a) Comparison of F_X between the pair-cat and the single-cat codes. (b) Probabilities of excitations out of the $\mathcal{C}$ and $\mathcal{C}_\mu$ subspaces, given respectively by $[1 - \langle \mathcal{C}_+^\beta|\rho|\mathcal{C}_+^\beta\rangle - \langle \mathcal{C}_-^\beta|\rho|\mathcal{C}_-^\beta\rangle]$ and $[1 - \langle \mu_+|\rho|\mu_+\rangle - \langle \mu_-|\rho|\mu_-\rangle]$ in the presence of decoherence. Other parameters are $\lambda = \Delta = 0.1$ K and $\tilde{\delta} = 0.01\Delta$. For the pair-cat code, we choose $\delta = 0$.

(dephasing) rate of the cavity mode j with $j = a,\ b$. Assuming $\kappa_j, \kappa_j^\phi \ll E_{\rm gap}$, the dynamics of the cat-state qubit is well confined to the subspace $\mathcal{C}$ because a stochastic jump does not cause leakage to the excited eigenstates for large β [33,34,36].

After a projection of the system onto the cat-state subspace $\mathcal{C}$, the effective master equation becomes (see details in the Supplemental Material [39])

$$\begin{aligned}\dot{\rho} \approx & -i[H_R, \rho] + \kappa \mathcal{D}[a]\rho + \kappa_a^\phi \mathcal{D}[a^\dagger a]\rho \\ & + \kappa_b |\beta|^2 \mathcal{D}\left[\frac{A + A^{-1}}{2}\sigma_x + \frac{A - A^{-1}}{2}\sigma_y\right]\rho \\ & + \kappa_b^\phi |\beta|^4 \mathcal{D}\left[\frac{A^2 + A^{-2}}{2}\mathbb{1}_\beta - \frac{A^2 - A^{-2}}{2}\sigma_z\right]\rho. \end{aligned} \tag{16}$$

For large β, the σ_y and σ_z terms are exponentially suppressed, leaving only the bit-flipping error σ_x. As shown in Fig. 7(b), when considering only single-photon losses, the probability to go out of the cat-state subspace is negligible (see the blue-dashed and red-solid curves). However, because $b^\dagger b|\pm\beta\rangle = \beta^2|\pm\beta\rangle \pm \beta D(\pm\beta)|1\rangle$, the leakage probability becomes proportional to $(\kappa_b^\phi \beta / E_{\rm gap})^2$ for pure dephasing (the green-hollow curve) [33,39]. To suppress such a leakage, the dephasing rate should be as small as possible for the simulation protocol.

For the pair-cat code, according to Eqs. (11) and (12), one can calculate that single-photon losses cannot induce leakage out of the computational subspace $\mathcal{C}_\mu$ when $\alpha = \beta \geq \sqrt{2}$. This is demonstrated with the brown-dashed-dotted curve in Fig. 6(b). Single-photon losses only induce bit-flip error. Similar to the case of a single-cat qubit, the pair-cat qubit is also robust against phase-flip error, as demonstrated in Eqs. (11) and (12). Though, the dephasing rates should be small to suppress the leakage probability. For instance, the leakage probability is about 0.5% when $\kappa_a^\phi = \kappa_b^\phi = 0.005\Delta$. Enlarging the amplitudes α and β can suppress the leakage probability because $a^\dagger a|\pm\alpha\rangle = \alpha^2|\pm\alpha\rangle \pm \alpha D(\pm\alpha)|1\rangle$ and $b^\dagger b|\pm\beta\rangle = \beta^2|\pm\beta\rangle \pm \beta D(\pm\beta)|1\rangle$ (see details in the Supplemental Material [39]). However, this increases the experimental difficulty in realizing the protocol.

Conclusions.—We have investigated how to amplify the coupling between a parametrically driven KNR (corresponding to a cat-state qubit) and cavity to effectively reach the USC. The bias-preserving character of the cat-state qubit makes the simulation protocol robust against the frequency mismatch and the amplitude mismatch of the parametric drive. Thus, a precise effective Hamiltonian can be obtained for exploring USC-induced quantum phenomena and applications, such as collapse and revivals of quantum states, pair-cat-code computation, as well as hidden symmetry and tunneling dynamics. Our numerical simulations show that this protocol can simulate the USC dynamics with high fidelity in the presence of parameter imperfections. We have applied the model for implementing a pair-cat code, which is a promising error-correction code because it meets the Knill-Laflamme condition better and preserves the noise bias stronger than a single-cat code. This allows us to reach the same level of protection of single-cat codes with a lower average photon number per mode. We can predict that further increasing the number of modes can further reduce the average photon number per mode to reach the same level of protection [53]. However, this may make the system too complicated to realize. In summery, our results open a path toward error-tolerant simulations of ultrastrong light matter couplings, as well as promising applications of error-correction qubits [30].

Y.-H. C. is supported by the National Natural Science Foundation of China under Grant No. 12304390. Y. X. is supported by the National Natural Science Foundation of China under Grant No. 11575045, the Natural Science Funds for Distinguished Young Scholar of Fujian Province under Grant No. 2020J06011 and Project from Fuzhou University under Grant No. JG202001-2. F. N. is supported in part by Nippon Telegraph and Telephone Corporation (NTT) Research, the Japan Science and Technology Agency (JST) [via the Quantum Leap Flagship Program (Q-LEAP), and the Moonshot R&D Grant No. JPMJMS2061], the Asian Office of Aerospace Research and Development (AOARD) (via Grant No. FA2386-20-1-4069), and the Office of Naval Research (ONR) (via Grant No. N62909-23-1-2074).

*Contact author: xia-208@163.com

[1] M. O. Scully and M. S. Zubairy, *Quantum Optics* (Cambridge University Press, Cambridge, England, 1997), 10.1017/cbo9780511813993.

[2] G. S. Agarwal, *Quantum Optics* (Cambridge University Press, Cambridge, England, 2012), 10.1017/cbo9781139035170.

[3] A. Auffeves *et al.*, *Strong Light-Matter Coupling: From Atoms to Solid-State Systems* (World Scientific, Singapore, 2013), 10.1142/8758.

[4] A. F. Kockum, A. Miranowicz, S. De Liberato, S. Savasta, and F. Nori, Ultrastrong coupling between light and matter, Nat. Rev. Phys. **1**, 19 (2019).

[5] P. Forn-Díaz, L. Lamata, E. Rico, J. Kono, and E. Solano, Ultrastrong coupling regimes of light-matter interaction, Rev. Mod. Phys. **91**, 025005 (2019).

[6] A. F. Kockum, A. Miranowicz, V. Macrì, S. Savasta, and F. Nori, Deterministic quantum nonlinear optics with single atoms and virtual photons, Phys. Rev. A **95**, 063849 (2017).

[7] P. Forn-Díaz, J. J. García-Ripoll, B. Peropadre, J.-L. Orgiazzi, M. A. Yurtalan, R. Belyansky, C. M. Wilson, and A. Lupascu, Ultrastrong coupling of a single artificial atom to an electromagnetic continuum in the nonperturbative regime, Nat. Phys. **13**, 39 (2016).

[8] F. Yoshihara, T. Fuse, S. Ashhab, K. Kakuyanagi, S. Saito, and K. Semba, Superconducting qubit–oscillator circuit beyond the ultrastrong-coupling regime, Nat. Phys. **13**, 44 (2016).

[9] F. Yoshihara, T. Fuse, S. Ashhab, K. Kakuyanagi, S. Saito, and K. Semba, Characteristic spectra of circuit quantum electrodynamics systems from the ultrastrong- to the deep-strong-coupling regime, Phys. Rev. A **95**, 053824 (2017).

[10] S. J. Bosman, M. F. Gely, V. Singh, A. Bruno, D. Bothner, and G. A. Steele, Multi-mode ultra-strong coupling in circuit quantum electrodynamics, npj Quantum Inf. **3**, 46 (2017).

[11] D. Ballester, G. Romero, J. J. García-Ripoll, F. Deppe, and E. Solano, Quantum simulation of the ultrastrong-coupling dynamics in circuit quantum electrodynamics, Phys. Rev. X **2**, 021007 (2012).

[12] W. Qin, A. Miranowicz, P.-B. Li, X.-Y. Lü, J. Q. You, and F. Nori, Exponentially enhanced light-matter interaction, cooperativities, and steady-state entanglement using parametric amplification, Phys. Rev. Lett. **120**, 093601 (2018).

[13] C. Leroux, L. C. G. Govia, and A. A. Clerk, Enhancing cavity quantum electrodynamics via antisqueezing: Synthetic ultrastrong coupling, Phys. Rev. Lett. **120**, 093602 (2018).

[14] C. Sánchez Muñoz, A. F. Kockum, A. Miranowicz, and F. Nori, Simulating ultrastrong-coupling processes breaking parity conservation in Jaynes-Cummings systems, Phys. Rev. A **102**, 033716 (2020).

[15] J. Braumüller, M. Marthaler, A. Schneider, A. Stehli, H. Rotzinger, M. Weides, and A. V. Ustinov, Analog quantum simulation of the Rabi model in the ultra-strong coupling regime, Nat. Commun. **8**, 779 (2017).

[16] D. Lv, S. An, Z. Liu, J.-N. Zhang, J. S. Pedernales, L. Lamata, E. Solano, and K. Kim, Quantum simulation of the quantum Rabi model in a trapped ion, Phys. Rev. X **8**, 021027 (2018).

[17] M.-L. Cai, Z.-D. Liu, W.-D. Zhao, Y.-K. Wu, Q.-X. Mei, Y. Jiang, L. He, X. Zhang, Z.-C. Zhou, and L.-M. Duan, Observation of a quantum phase transition in the quantum Rabi model with a single trapped ion, Nat. Commun. **12**, 1126 (2021).

[18] X. Chen, Z. Wu, M. Jiang, X.-Y. Lü, X. Peng, and J. Du, Experimental quantum simulation of superradiant phase transition beyond no-go theorem via antisqueezing, Nat. Commun. **12**, 6281 (2021).

[19] R.-H. Zheng, W. Ning, Y.-H. Chen, J.-H. Lü, L.-T. Shen, K. Xu, Y.-R. Zhang, D. Xu, H. Li, Y. Xia, F. Wu, Z.-B. Yang, A. Miranowicz, N. Lambert, D. Zheng, H. Fan, F. Nori, and S.-B. Zheng, Observation of a superradiant phase transition with emergent cat states, Phys. Rev. Lett. **131**, 113601 (2023).

[20] I. M. Georgescu, S. Ashhab, and F. Nori, Quantum simulation, Rev. Mod. Phys. **86**, 153 (2014).

[21] W. Qin, A. F. Kockum, C. Sánchez Muñoz, A. Miranowicz, and F. Nori, Quantum amplification and simulation of strong and ultrastrong coupling of light and matter, Phys. Rep. **1078**, 1 (2024).

[22] S. Ashhab and F. Nori, Qubit-oscillator systems in the ultrastrong-coupling regime and their potential for preparing nonclassical states, Phys. Rev. A **81**, 042311 (2010).

[23] X. Cao, J. Q. You, H. Zheng, and F. Nori, A qubit strongly coupled to a resonant cavity: Asymmetry of the spontaneous emission spectrum beyond the rotating wave approximation, New J. Phys. **13**, 073002 (2011).

[24] Y.-H. Chen, W. Qin, X. Wang, A. Miranowicz, and F. Nori, Shortcuts to adiabaticity for the quantum Rabi model: Efficient generation of giant entangled cat states via parametric amplification, Phys. Rev. Lett. **126**, 023602 (2021).

[25] S. C. Burd, R. Srinivas, H. M. Knaack, W. Ge, A. C. Wilson, D. J. Wineland, D. Leibfried, J. J. Bollinger, D. T. C. Allcock, and D. H. Slichter, Quantum amplification of boson-mediated interactions, Nat. Phys. **17**, 898 (2021).

[26] T. C. Ralph, A. Gilchrist, G. J. Milburn, W. J. Munro, and S. Glancy, Quantum computation with optical coherent states, Phys. Rev. A **68**, 042319 (2003).

[27] A. Gilchrist, K. Nemoto, W. J. Munro, T. C. Ralph, S. Glancy, S. L. Braunstein, and G. J. Milburn, Schrödinger cats and their power for quantum information processing, J. Opt. B **6**, S828 (2004).

[28] M. Mirrahimi, Z. Leghtas, V. V. Albert, S. Touzard, R. J. Schoelkopf, L. Jiang, and M. H. Devoret, Dynamically protected cat-qubits: A new paradigm for universal quantum computation, New J. Phys. **16**, 045014 (2014).

[29] M. Mirrahimi, Cat-qubits for quantum computation, C.R. Phys. **17**, 778 (2016).

[30] S. M. Girvin, Introduction to quantum error correction and fault tolerance, SciPost Phys. Lect. Notes 70 (2023).

[31] W. Cai, Y. Ma, W. Wang, C.-L. Zou, and L. Sun, Bosonic quantum error correction codes in superconducting quantum circuits, Fund. Res. **1**, 50 (2021).

[32] W.-L. Ma, S. Puri, R. J. Schoelkopf, M. H. Devoret, S. M. Girvin, and L. Jiang, Quantum control of bosonic modes with superconducting circuits, Sci. Bull. **66**, 1789 (2021).

[33] S. Puri, A. Grimm, P. Campagne-Ibarcq, A. Eickbusch, K. Noh, G. Roberts, L. Jiang, M. Mirrahimi, M. H. Devoret, and S. M. Girvin, Stabilized cat in a driven nonlinear cavity: A fault-tolerant error syndrome detector, Phys. Rev. X **9**, 041009 (2019).

[34] S. Puri, L. St-Jean, J. A. Gross, A. Grimm, N. E. Frattini, P. S. Iyer, A. Krishna, S. Touzard, L. Jiang, A. Blais, S. T. Flammia, and S. M. Girvin, Bias-preserving gates with stabilized cat qubits, Sci. Adv. **6**, eaay5901 (2020).

[35] A. Grimm, N. E. Frattini, S. Puri, S. O. Mundhada, S. Touzard, M. Mirrahimi, S. M. Girvin, S. Shankar, and M. H. Devoret, Stabilization and operation of a Kerr-cat qubit, Nature (London) **584**, 205 (2020).

[36] Y.-H. Chen, R. Stassi, W. Qin, A. Miranowicz, and F. Nori, Fault-tolerant multiqubit geometric entangling gates using photonic cat-state qubits, Phys. Rev. Appl. **18**, 024076 (2022).

[37] S. Puri, S. Boutin, and A. Blais, Engineering the quantum states of light in a Kerr-nonlinear resonator by two-photon driving, npj Quantum Inf. **3**, 18 (2017).

[38] Z. Wang, M. Pechal, E. A. Wollack, P. Arrangoiz-Arriola, M. Gao, N. R. Lee, and A. H. Safavi-Naeini, Quantum dynamics of a few-photon parametric oscillator, Phys. Rev. X **9**, 021049 (2019).

[39] See Supplemental Material at http://link.aps.org/supplemental/10.1103/PhysRevLett.133.033603 which include Refs. [40,41] for detailed derivations and discussions of our main results.

[40] J. Koch, T. M. Yu, J. Gambetta, A. A. Houck, D. I. Schuster, J. Majer, A. Blais, M. H. Devoret, S. M. Girvin, and R. J. Schoelkopf, Charge-insensitive qubit design derived from the Cooper pair box, Phys. Rev. A **76**, 042319 (2007).

[41] J. Q. You, X. Hu, S. Ashhab, and F. Nori, Low-decoherence flux qubit, Phys. Rev. B **75**, 140515(R) (2007).

[42] A. S. Darmawan, B. J. Brown, A. L. Grimsmo, D. K. Tuckett, and S. Puri, Practical quantum error correction with the XZZX code and Kerr-cat qubits, PRX Quantum **2**, 030345 (2021).

[43] Q. Xu, H. Putterman, J. K. Iverson, K. Noh, O. J. Painter, F. G. S. L. Brandao, and L. Jiang, *Quantum Computing, Communication, and Simulation II*, edited by P. R. Hemmer and A. L. Migdall (SPIE, San Francisco, 2022).

[44] J. Casanova, G. Romero, I. Lizuain, J. J. García-Ripoll, and E. Solano, Deep strong coupling regime of the Jaynes-Cummings model, Phys. Rev. Lett. **105**, 263603 (2010).

[45] M. Wakayama, Symmetry of asymmetric quantum Rabi models, J. Phys. A **50**, 174001 (2017).

[46] S. Ashhab, Attempt to find the hidden symmetry in the asymmetric quantum Rabi model, Phys. Rev. A **101**, 023808 (2020).

[47] Z.-M. Li and M. T. Batchelor, Hidden symmetry and tunneling dynamics in asymmetric quantum Rabi models, Phys. Rev. A **103**, 023719 (2021).

[48] L. Duan, S. He, D. Braak, and Q.-H. Chen, Solution of the two-mode quantum Rabi model using extended squeezed states, Europhys. Lett. **112**, 34003 (2015).

[49] E. K. Irish, J. Gea-Banacloche, I. Martin, and K. C. Schwab, Dynamics of a two-level system strongly coupled to a high-frequency quantum oscillator, Phys. Rev. B **72**, 195410 (2005).

[50] C. H. Bennett, D. P. DiVincenzo, J. A. Smolin, and W. K. Wootters, Mixed-state entanglement and quantum error correction, Phys. Rev. A **54**, 3824 (1996).

[51] E. Knill and R. Laflamme, Theory of quantum error-correcting codes, Phys. Rev. A **55**, 900 (1997).

[52] P. Zanardi and D. A. Lidar, Purity and state fidelity of quantum channels, Phys. Rev. A **70**, 012315 (2004).

[53] V. V. Albert, S. O. Mundhada, A. Grimm, S. Touzard, M. H. Devoret, and L. Jiang, Pair-cat codes: Autonomous error-correction with low-order nonlinearity, Quantum Sci. Technol. **4**, 035007 (2019).